Article:
Evans, C.A., Indjin, D., Ikonic, Z. et al. (2008) Thermal modeling of terahertz quantum-cascade lasers: comparison of optical waveguides. IEEE Journal of Quantum Electronics, 44 (7). pp. 680-685. ISSN: 0018-9197

https://doi.org/10.1109/JQE.2008.922327

Thermal Modeling of Terahertz Quantum-Cascade Lasers: Comparison of Optical Waveguides

Craig A. Evans, Dragan Indjin, Zoran Ikonić, Paul Harrison, *Senior Member, IEEE*, Miriam Serena Vitiello, Vincenzo Spagnolo, and Gaetano Scamarcio, *Member, IEEE*

***Abstract*—We compare a set of experimental lattice temperature profiles measured in a surface-emitting terahertz (THz) quantum-cascade laser (QCL) with the results of a 2-D anisotropic heat diffusion model. We evaluate the temperature dependence of the cross-plane thermal conductivity $(\kappa_\perp)$ of the active region which is known to be strongly anisotropic due to its superlattice-like nature. Knowledge of $\kappa_\perp$ and its temperature dependence is crucial in order to improve the temperature performance of THz QCLs and this has been used to investigate the longitudinal lattice temperature distribution of the active region and to compare the thermal properties of metal-metal and semi-insulating surface-plasmon THz optical waveguides using a 3-D anisotropic heat diffusion model.**

***Index Terms*—Optical waveguide, quantum-cascade laser (QCL), terahertz (THz), thermal conductivity, thermal modeling.**

I. Introduction

TERAHERTZ (THz) quantum-cascade lasers (QCLs) have shown a considerable increase in performance since their first demonstration [1], covering the frequency range 1.2–4.9 THz [2], [3] (and down to 0.83 THz with the assistance of a magnetic field [4]) with maximum operating temperatures of 117 K in continuous-wave (CW) and 164 K in pulsed-mode [5]. Improving the maximum operating temperatures of THz QCLs still further is highly attractive for a range of technological applications. This is made inherently more difficult in the THz frequency range than in the mid-infrared (MIR) due to the smaller photon energy (typically less than 20 meV). At higher lattice temperatures (and, hence, higher electron temperatures), it becomes more difficult to achieve selective injection and depopulation of the upper and lower laser levels. Additionally, since the photon energy is less than the LO phonon energy (36 meV in GaAs) in the THz frequency range, at sufficiently high electron temperatures, thermally activated LO phonon emission from the upper laser level can significantly reduce the population inversion.

In order to reduce the electron temperature and improve the temperature performance, the lattice temperature itself must be reduced through careful thermal management. Heat extraction from QCLs is difficult due to the large amounts of electrical power (P) dissipated in the device active regions, the poor thermal coupling of the active region with the heat sink which is determined by the waveguide and mounting configurations and, most importantly, the low thermal conductivity of the active region.

Due to its superlattice-like nature, the thermal conductivity of the QCL active region is strongly anisotropic and as a result, both the in-plane $(\kappa_{||})$ and cross-plane $(\kappa_\perp)$ thermal conductivities are reduced compared to the bulk values of the constituent materials. Since the layer widths are comparable to or less than the phonon mean free path, the phonon scattering rate at the interfaces between layers increases, hindering the phonon transport [6], [7]. The partially diffuse scattering of phonons at the interfaces can explain the reduction in $\kappa_{||}$ [8], while the stronger reduction in $\kappa_\perp$ is caused by the multiple reflections of phonons at the many interfaces [7]. Furthermore, THz QCLs particularly suffer compared to MIR devices since they generally contain more active region periods resulting in a larger number of interfaces and a higher value of thermal resistance (R_{TH}). It has been found that the interface contribution to the overall thermal resistivity of the THz QCLs can be as high as 97% [9].

The configuration of the optical waveguide also plays an important role in determining the thermal performance of the device and to date, two types of THz optical waveguides have been implemented: semi-insulating surface-plasmon (SISP) [1] and metal–metal (MM) waveguides [10]. SISP waveguides achieve optical confinement through the merging into a single mode of two surface plasmons bound at the interfaces between a highly doped semiconductor layer and a metallic layer which sandwich the semiconductor active region. On the other hand, MM waveguides are essentially the same as microstrip transmission lines which are widely used at microwave and millimeter-wave frequencies and THz QCLs utilizing this type of waveguide have proven to have to highest operating temperatures thus far [5].

It is clear that in order to understand the internal thermal dynamics of QCLs with the aim of improving temperature performance, knowledge of the temperature dependence of the active region thermal conductivity and the effect of the optical waveguide on the device thermal properties is crucial. In this paper we present a study of the local lattice temperature of a surface-emitting distributed-feedback (DFB) THz QCL which

Manuscript received October 30, 2007; revised Febuary 27, 2008. This work was supported in part by the EPSRC. The work of M. S. Vitiello, V. Spagnolo, and G. Scamarcio was supported in part by the Region Puglia PE-056 project.

C. A. Evans, D. Indjin, Z. Ikonić, and P. Harrison are with the Institute of Microwaves and Photonics, School of Electronic and Electrical Engineering, University of Leeds, Leeds LS2 9JT, U.K. (e-mail: c.a.evans@leeds.ac.uk).

M. S. Vitiello and G. Scamarcio are with the CNR-INFM Regional Laboratory LIT^3 and Dipartimento Interateneo di Fisica "M.Merlin," Universitá degli Studi di Bari, 70126 Bari, Italy (e-mail: vitiello@fisica.uniba.it; scamarcio@fisica.uniba.it).

V. Spagnolo is with the CNR-INFM Regional Laboratory LIT^3 and Dipartimento Interateneo di Fisica "M.Merlin", Politecnico di Bari, 70126 Bari, Italy.

Digital Object Identifier 10.1109/JQE.2008.922327

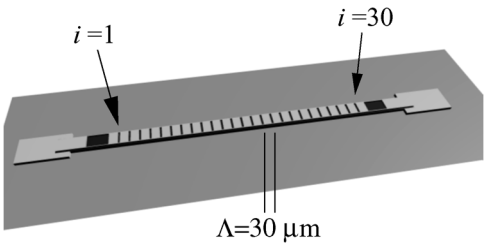

Fig. 1. Schematic representation of the device (not to scale) labelling the apertures and the grating period.

lases in pulsed mode up to 149 K [11], measured using a microprobe photoluminescence (PL) technique [12], [13]. The studied device emits at ∼3 THz utilizing the same resonant-phonon depopulation active region as in [5]. The threshold current density at 5 K was measured to be 460 A/cm^2 and lasing ceases at a bias of ∼15 V [11].

The paper is organized as follows. The experimental procedure is outlined in Section II and the extracted values of $R_{\rm TH}$ presented. In Section III, the development of an anisotropic thermal model of heat diffusion in QCLs is presented together with temperature-dependent material parameters. Section IV details the use of the thermal model in conjunction with the experimental results in order to extract the temperature-dependence of $\kappa_\perp$. In Section V, the thermal properties of SISP and MM waveguides are analyzed and compared and in Section VI, the longitudinal temperature distribution in a THz QCL waveguide is investigated. Finally, we draw conclusions from our results.

II. Experimental Procedure and Results

A microprobe band-to-band PL technique was used to measure the local lattice temperature (T_L) of the surface-emitting THz QCL. By measuring the energy of the main PL peak and comparing the shift to calibration curves obtained when probing the device at zero current while varying the heat sink temperature T_H it is possible to extract T_L. Whereas in our previous works we have measured the facet temperatures of various THz and MIR devices [12]–[16], the use of a surface-emitting device allows T_L to be measured on top of the device active region through the apertures in the second-order DFB grating [9]. The investigated sample has an active region thickness of $d = 10$ μm, a ridge width of 45 μm and a cavity length of 1.14 mm. The optical confinement is provided by a MM waveguide fabricated with Cu–Cu bonding. The second-order DFB grating is composed of $i = 1$ to 30 apertures, each 6 μm wide with a grating period of $\Lambda = 30$ μm. A schematic representation of the device is shown in Fig. 1.

Fig. 2 shows the local lattice temperature (T_L) measured in the center of the central $(i = 15)$ aperture as a function of electrical power P at a heat sink temperature $T_H = 75$ K. Since T_L has been measured on top of the laser ridge, which is the hottest region of the device, from the experimental data of Fig. 2 we

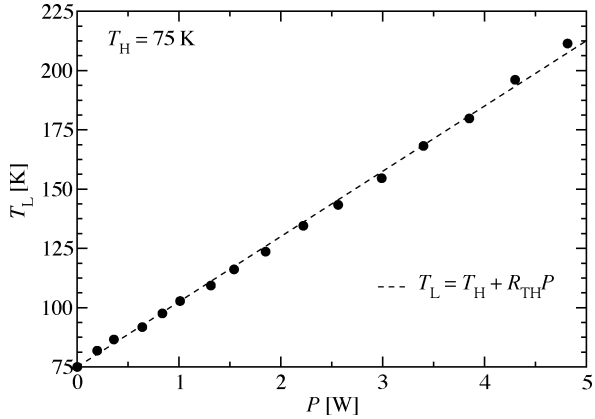

Fig. 2. Local lattice temperature (T_L) measured in the central aperture of the surface-emitting THz QCL as a function of electrical power (P)[Data from [9]]. The dashed line shows a linear fit to the data according to the relation $(T_L = T_H + R_{\rm TH}P)$ from which a device thermal resistance of $R_{\rm TH} = 27.8 \pm 0.2$ K/W is extracted. All measurements were performed at $T_H = 75$ K.

can extract the device thermal resistance $R_{\rm TH}$, according to the relation

$$R_{\rm TH} = \frac{T_L - T_H}{P}. \tag{1}$$

We found $R_{\rm TH} = 27.8 \pm 0.2$ K/W.

III. Theoretical Framework

A. Model Development

In order to calculate the active region temperature, a steady-state anisotropic thermal model of heat diffusion in QCLs is employed which is based upon Fourier's heat equation

$$\nabla \cdot [\kappa \nabla T] + Q = 0 \tag{2}$$

where κ is the thermal conductivity tensor, T is the temperature, and Q is the heat generated per unit volume. As in our previous work [17], we solve (2) using a finite-difference (FD) approach. The spatial domain where the solution is sought is discretized into a non-overlapping grid and (2) is solved at the nodes with appropriate continuity of the solution across the interfaces between the nodes and subject to relevant boundary conditions at the domain edge. Equation (2) itself is discretized onto the computational grid and in the 3-D case it is generalized to

$$\nabla \cdot \left(\begin{bmatrix} \kappa_x & 0 & 0 \\ 0 & \kappa_y & 0 \\ 0 & 0 & \kappa_z \end{bmatrix} \cdot \nabla T \right) + Q = 0 \tag{3}$$

where κ_x, κ_y, and κ_z are the x-, y-, and z-components of the anisotropic thermal conductivity, respectively. Only the superlattice-like QCL active region has an anisotropic thermal conductivity and in this layer κ_y (κ_x and κ_z) is equivalent to $\kappa_\perp$ $(\kappa_{||})$. The remaining layers in the device are isotropic hence $\kappa_x = \kappa_y = \kappa_z$ and are given by the appropriate bulk thermal conductivities. In this work, it is approximated that all the input electrical power is dissipated as heat in the device active region and resistive heating in all other layers is ignored.

TABLE I
TEMPERATURE DEPENDENT LATTICE THERMAL CONDUCTIVITIES USED IN THE SIMULATIONS

Material	Lattice thermal conductivity [W m^{-1} K^{-1}]
GaAs	$74500T^{-1.30}$ [18]
AlAs	$225270T^{-1.37}$ [19]
Au	$337 - 6.6 \times 10^{-2}T$ [20]
SiO_2	$9.75 \times 10^{-4} + 5.38 \times 10^{-5}T - 4.69 \times 10^{-8}T^2$ [21]

Equation (3) is expanded and the derivatives replaced by central FD approximations. The nodal temperatures are then calculated using a successive over-relaxation (SOR) technique. The temperature at the bottom of the substrate is fixed at the constant heat sink temperature and Neumann (zero-derivative) boundary conditions are used at all other surfaces. In order to reduce the memory requirements and CPU run-time, a Neumann boundary condition can be applied to any symmetry plane in the structure to reduce the number of nodes by factor of two. In the 3-D case, the device has symmetry planes at the center of the ridge both longitudinally and laterally, meaning it suffices to calculate the temperature distribution in only one quarter of the structure, reducing the computational grid by a factor of four.

B. Material Parameters

For increased accuracy, the model takes into account the temperature dependent lattice thermal conductivities of the materials in the device. Table I lists the temperature dependent lattice thermal conductivities used in the simulations. As well as being temperature dependent, the lattice thermal conductivity of a semiconductor also depends upon the doping level and decreases by 8% per decade starting from 10^{15} cm^{-3} [22] due to the influence of the ionized impurities on the phonon transport. Therefore, the values of lattice thermal conductivity listed in Table I are scaled according to the doping level of each particular layer in the simulated structure. We have estimated the electronic contribution to the thermal conductivity using the Weidemann–Franz law and found it to be negligible compared to the lattice thermal conductivity and it is therefore ignored in this work.

When calculating the thermal conductivity of the ternary $Al_{0.15}Ga_{0.85}As$ alloy, Abele's interpolation scheme is used, i.e.,

$$\frac{1}{k_{A_xB_{1-x}C}} = \frac{x}{k_{AC}} + \frac{1-x}{k_{BC}} + \frac{x(1-x)}{C_{AB}} \tag{4}$$

where in the case of the $Al_{0.15}Ga_{0.85}As$ alloy, the bowing parameter C_{AB} is 3.33 W $\cdot$ m^{-1} $\cdot$ K^{-1} [18]. As discussed in Section I, $\kappa_{||}$ is reduced compared to bulk due to partially diffusive scattering of phonons at the interfaces and in this work we use a value corresponding to 75% of the weighted average of the GaAs and $Al_{0.15}Ga_{0.85}As$ in the active region (equivalent to an Al fraction of $x = 0.02$) [20].

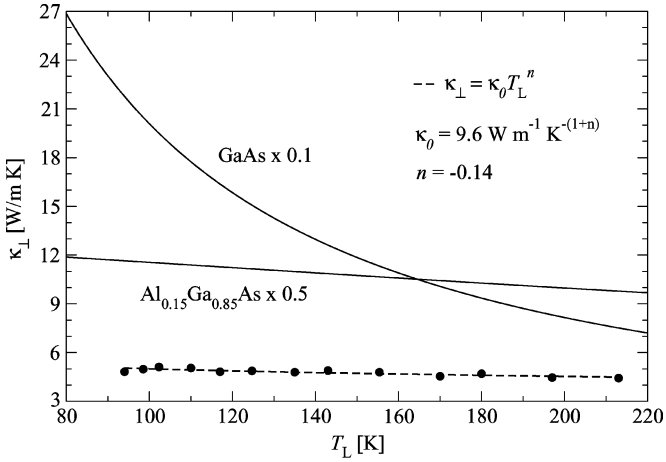

Fig. 3. Cross-plane thermal conductivity ($\kappa_\perp$) of the active region as a function of temperature extracted from fitting the results of the 2-D thermal model to the experimental data presented in Fig. 2. The dashed line is a power law fit to the data, $9.6T^{-0.14}$ W $\cdot$ m^{-1} $\cdot$ K^{-1}. For comparison, the solid lines shows the thermal conductivities of bulk GaAs and $Al_{0.15}Ga_{0.85}As$.

IV. EXTRACTION OF THE CROSS-PLANE THERMAL CONDUCTIVITY

In order to fully understand the thermal dynamics of QCLs and improve their temperature performance, knowledge of $\kappa_\perp$ and its dependence on temperature is crucial. In this section, the model described in Section III is employed in conjunction with the experimental data of Section II to extract $\kappa_\perp$ and its temperature dependence. A 2-D cross section of the device taken from the center of the laser cavity was simulated for each of the electrical powers in Fig. 2 at $T_H = 75$ K with $\kappa_\perp$ the only fitting parameter. By matching the value of $\kappa_\perp$ in the simulations that causes the same temperature rise as measured for each power in Fig. 2, it is possible to extract $\kappa_\perp$ as a function of temperature and the results are shown in Fig. 3. The same power law ($\kappa = \kappa_0 T^n$) that is used for bulk semiconductors is used to fit the data and values of $\kappa_0 = 9.6$ W $\cdot$ m^{-1} $\cdot$ K$^{-(1+n)}$ and $n = -0.14$ are extracted. The results show that $\kappa_\perp$ is a decreasing function of temperature with a much weaker temperature dependence than III–V bulk semiconductors, where n is found to be typically in the range $-1.55 \leq n \leq -1.20$ [18]. The values of $\kappa_\perp$ extracted here are in good agreement with experimentally measured values of the cross-plane thermal conductivity of standard edge-emitting THz QCLs ($\kappa_0 = 10.6$ W $\cdot$ m^{-1} $\cdot$ K$^{-(1+n)}$, $n = -0.16$) [23] and GaAs–AlAs superlattices [7]. Also shown in Fig. 3 for comparison are the thermal conductivities of bulk GaAs and $Al_{0.15}Ga_{0.85}As$ which are much larger than $\kappa_\perp$, a trend which has previously been observed in the GaAs–AlGaAs [24], GaInAs–AlInAs [13], [20], and Si–SiGe [25] material systems.

It is worth noting that as opposed to the decrease of $\kappa_\perp$ with temperature in GaAs–Al(Ga)As superlattices, in the GaInAs–AlInAs and Si–SiGe material systems, $\kappa_\perp$ is found to increase with temperature [13], [20], [25]. At present, no satisfactory explanation for this behavior exists [6], [7]. Possible explanations are better quality growth (due to the extremely small lattice mismatch) and a smaller 'acoustic mismatch' in GaAs-based superlattices [26], [27].

V. Comparison of the Thermal Properties of Different Optical Waveguides

The optical waveguide is an integral component of a THz QCL and in order to increase the maximum operating temperature it is important to understand the effect of the waveguide on the thermal properties of the QCL. Similar studies have recently been carried out on InP-based midinfrared devices [28]. This Section presents a comparison between the thermal properties of MM and SISP optical waveguides and the effect on device performance.

In the following simulations, the MM optical waveguide is taken to have the same dimensions as the one in Section II (45-μm-wide laser ridge and a 1.14-mm-long cavity) with $d = 10$ μm and a 160-μm-thick substrate but without the apertures in the top contact. In order to make the comparison more meaningful, the SISP waveguide is taken to be similar to the one in [29] (150-μm-wide laser ridge and a 2-mm-long cavity) but with the same active region and substrate thicknesses as the MM waveguide. In the case of the SISP waveguide, the substrate is semi-insulating while the MM waveguide substrate is n^+ doped at 2×10^{18} cm^{-3}. In both cases, the $\kappa_\perp$ values extracted in Section IV are used together with the temperature-dependent thermal conductivity values given in Section III-B, correctly adjusted for the doping level. At $T_H = 75$ K, $R_{\rm TH} = 20.7$ K/W for the MM waveguide, in reasonable agreement with the experimentally measured value of 27.8 K/W in Section II. The discrepancy in values is due to lack of the apertures in the simulated MM device which were present in the measured device.

When comparing the thermal resistances of MM and SISP waveguides, it is important to take into account the variation of the device dimensions. Due to the strong optical confinement in MM waveguides, the laser ridge can be sub-wavelength in width as opposed to SISP waveguides and in order to take this into account, the thermal resistances of the two waveguides have been normalized according to $R^*_{\rm TH} = R_{\rm TH}\times A/d$ where A is the area of the laser ridge. The use of this scaling factor is justified since in THz QCL waveguides the heat diffusion can be considered 1-D due to the uncovered ridge sidewalls which mean that heat can only escape the active region vertically. We have performed simulations (not presented) which show that variations in $R^*_{\rm TH}$ are less than $\sim$1% ($\sim$5%) when the ridge thickness (width) are both doubled and halved. Simulations were performed over a range of electrical powers at various values of T_H and $R_{\rm TH}$ extracted according to (1). The results for both $R^*_{\rm TH}$ and $R_{\rm TH}$ are plotted in Fig. 4 as a function of T_H. The results shows that at low heat sink temperatures, the normalized thermal resistance of the MM waveguide is higher than that of the SISP waveguide and above $T_H \sim 35$ K the normalized thermal resistance of the SISP waveguide becomes the highest and the difference between the two continues to increase as T_H increases. This behaviour is explained by the different substrates and bottom contact layers in each of the waveguides. In all cases $R_{\rm TH}$ of the MM waveguide is greater than that of the SISP waveguide due to its smaller area.

Below this threshold temperature, the total thermal resistance of the SI substrate and n^+ bottom contact layer in the SISP waveguide is less than that of the n^+ substrate and the Cu bottom contact layer in the MM waveguide. The n^+ substrate in the MM waveguide is the major contributor to this behaviour. Beyond the critical temperature, the reduced thermal conductivity of the n^+ bottom contact layer in the SISP waveguide compared to the Cu bottom contact layer in the MM waveguide becomes the major contributor and the normalized thermal resistance of the MM waveguide is therefore lower than that of the SISP waveguide. Since one of the major goals of research into THz QCLs is to increase the temperature performance (at least up to temperatures accessible by thermo-electric coolers), these results confirm that MM waveguides offer the best route for achieving this goal. It should be noted that MM waveguides often exhibit smaller threshold current densities than SISP waveguide due to their unity mode confinement factor and reduced mirror losses [30] which lead to smaller amounts of dissipated electrical power and this factor also contributes to their superior thermal performance.

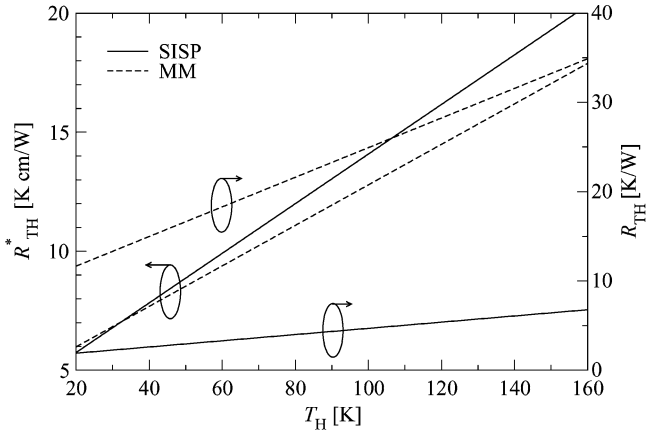

Fig. 4. Calculated thermal resistance $R_{\rm TH}$ and normalized thermal resistance $R^*_{\rm TH}$ as a function of T_H for both the SISP and MM optical waveguides.

VI. Investigation of the Longitudinal Temperature Distribution

In our previous works, we have measured the temperature profiles on the laser facets of various THz and MIR QCLs [12]–[16], however in this Section we investigate the temperature distribution along the length of the laser ridge in the surface-emitting THz QCL. Fully 3-D simulations have been performed using the thermal model outlined in Section III. The longitudinal temperature distribution is extracted from the top of the active region along the center of the laser ridge, where the measurements in Section II were taken. Fig. 5 shows the simulated longitudinal temperature distribution at the center of the ridge along one half of the cavity length at $T_H = 75$ K for $P = 2.1$ and 4 W. The results show that along the length of the laser cavity where the apertures exist, T_L remains approximately constant, with the temperature in the central $(i = 15)$ aperture being slightly higher ($\sim$3 K) than the temperature in the aperture at the end of the cavity $(i = 1)$. These results are in excellent agreement with experimentally measured values on the same device [9]. In the surface-emitting THz QCL, bond pads are fabricated at the ends of the cavity that also cover the electrically insulated ends of the cavity while the sidewalls are

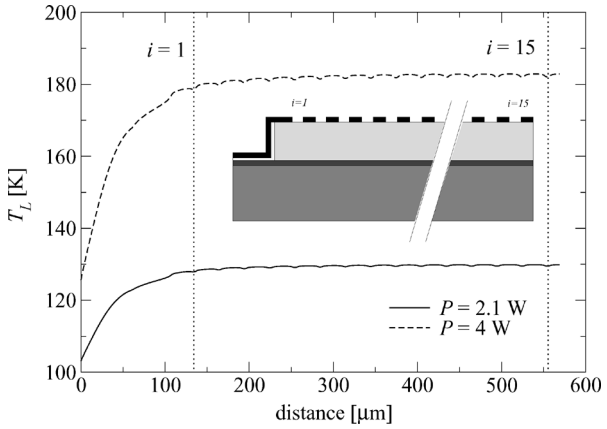

Fig. 5. Simulated longitudinal temperature distribution at the center of the ridge along the laser cavity of the surface-emitting THz QCL at $T_H = 75$ K for $P = 2.1$ W (solid line) and 4 W (dashed line). The dotted lines show the locations of the first ($i = 1$) and central ($i = 15$) apertures in the DFB grating. Close to the ends of the laser cavity, T_L is reduced due to longitudinal heat escape channels formed by the insulator/metallic coating on the laser facets. The inset shows a schematic cross section along the length of the surface-emitting THz QCL (not to scale).

left uncoated [11]. This configuration opens up longitudinal heat escape channels which take advantage of the fact $\kappa_{||} > \kappa_{\perp}$ and hence T_L decreases near to the ends of the laser cavity. This effect is particular to this type of device as in standard edge-emitting QCLs, the laser facets at the ends of the cavity are uncoated and hence no longitudinal heat channels will exist and the temperature can be expected to be constant along the length of the laser cavity.

These results suggest the possibility of reducing T_L by covering the sidewalls of the ridge (with sufficient electrical insulation) with gold in order to open up lateral heat escape channels. This approach has proved extremely successful in midinfrared InP-based QCLs [31].

VII. Conclusion

We used the longitudinal local lattice temperatures measured in a surface-emitting THz QCL [9] in conjunction with an anisotropic thermal model of heat diffusion in QCLs to extract temperature dependent values of $\kappa_{\perp}$. The values are found to be a decreasing function of temperature an order of magnitude smaller than the equivalent bulk alloy and are in excellent agreement with experimentally measured values for GaAs–AlAs superlattices and similar THz QCL active regions.

We have compared the thermal properties of SISP and MM THz optical waveguides. It has been found that at low lattice temperatures the thermal resistance of SISP waveguides is lower than MM waveguides, due to the higher thermal conductivity of its semi-insulating substrate compared to the highly doped substrate of the MM waveguide. At higher temperatures, the thermal resistance of the MM waveguide is the lowest and the difference between the two continues to become larger as the heat sink temperature is increased. This confirms that MM optical waveguide offer to best route for increasing the maximum operating temperature of THz QCLs.

The longitudinal temperature distribution in the surface-emitting THz QCL has been investigated. The temperature is found to be approximately constant along the length of the cavity accessible by the apertures in the DFB with the temperature in the center being a few kelvins higher than at the edge, in good agreement with experimentally measured values.

References

[1] R. Köhler, A. Tredicucci, F. Beltram, H. E. Beere, E. H. Linfield, A. G. Davies, D. A. Ritchie, R. C. Iotti, and F. Rossi, "Terahertz semiconductor heterostructure laser," *Nature*, vol. 417, no. 156, pp. 156–159, 2002.

[2] C. Walther, M. Fischer, G. Scalari, R. Terazzi, N. Hoyler, and J. Faist, "Quantum cascade lasers operating from 1.2 to 1.6 THz," *Appl. Phys. Lett.*, vol. 91, no. 131122, pp. 1–3, 2007.

[3] A. W. M. Lee, Q. Qin, S. Kumar, B. S. Williams, Q. Hu, and J. L. Reno, "Real-time terahertz imaging over a standoff distance (>25 meters)," *Appl. Phys. Lett.*, vol. 89, no. 141125, pp. 1–3, 2006.

[4] G. Scalari, C. Walther, J. Faist, H. E. Beere, and D. A. Ritchie, "Laser emission at 830 and 960 GHz from quantum cascade structures," presented at the ITQW2007, Ambleside, U.K., Sep. 10–14, 2007, unpublished.

[5] B. S. Williams, S. Kumar, Q. Hu, and J. L. Reno, "Operation of terahertz quantum-cascade lasers at 164 K in pulsed mode and at 117 K in continuous-wave mode," *Opt. Exp.*, vol. 13, no. 9, p. 3331, 2005.

[6] G. Chen, "Thermal conductivity and ballistic-phonon transport in the cross-plane direction of superlattices," *Phys. Rev. B*, vol. 57, pp. 14958–14973, 1998.

[7] W. S. Capinski, H. J. Maris, T. Ruf, M. Cardona, K. Ploog, and D. S. Katzer, "Thermal-conductivity measurements of GaAs–AlAs superlattices using a picosecond optical pump-and-probe technique," *Phys. Rev. B*, vol. 59, pp. 8105–8113, 1999.

[8] G. Chen and M. Neagu, "Thermal conductivity and heat transfer in superlattices," *Appl. Phys. Lett.*, vol. 71, pp. 2761–2763, 1997.

[9] G. Scamarcio, M. S. Vitiello, V. Spagnolo, S. Kumar, B. S. Williams, and Q. Hu, "Nanoscale heat transfer in quantum cascade lasers," *Physica E*, vol. 40, no. 6, p. 1780, 2008.

[10] B. S. Williams, S. Kumar, H. Callebaut, and Q. Hu, "Terahertz quantum-cascade laser at $\lambda \approx 100$ μm using metal waveguide for mode confinement," *Appl. Phys. Lett.*, vol. 83, no. 11, pp. 2124–2126, 2003.

[11] S. Kumar, B. S. Williams, Q. Qin, A. W. M. Lee, Q. Hu, and J. L. Reno, "Surface-emitting distributed feedback terahertz quantum-cascade lasers in metal-metal waveguides," *Opt. Exp.*, vol. 15, no. 1, p. 113, 2007.

[12] V. Spagnolo, M. Troccoli, G. Scamarcio, C. Gmachl, F. Capasso, A. Tredicucci, A. M. Sergent, A. L. Hutchinson, D. L. Sivco, and A. Y. Cho, "Temperature profile of GaInAs–AlInAs–InP quantum cascade-laser facets measured by microprobe photoluminescence," *Appl. Phys. Lett.*, vol. 78, no. 15, p. 2095, 2001.

[13] V. Spagnolo, G. Scamarcio, D. Marano, M. Troccoli, F. Capasso, C. Gmachl, A. M. Sergent, A. L. Hutchinson, D. L. Sivco, A. Y. Cho, H. Page, C. Becker, and C. Sirtori, "Thermal characteristics of quantum-cascade lasers by micro-probe optical spectroscopy," *Proc. IEE Optoelectron.*, vol. 150, no. 4, p. 298, 2003.

[14] M. S. Vitiello, G. Scamarcio, V. Spagnolo, A. Lops, Q. Yang, C. Manz, and J. Wagner, "Experimental investigation of the lattice and electronic temperatures in $Ga_{0.47}In_{0.53}As$–$Al_{0.62}Ga_{0.38}As_{1-x}Sb_x$ quantum-cascade lasers," *Appl. Phys. Lett.*, vol. 90, no. 121109, pp. 1–3, 2007.

[15] M. S. Vitiello, V. Spagnolo, G. Scamarcio, J. Alton, S. Barbieri, C. Worrall, H. E. Beere, D. A. Ritchie, and C. Sirtori, "Thermal properties of THz quantum cascade lasers based on different optical waveguide configurations," *Appl. Phys. Lett.*, vol. 89, no. 021111, pp. 1–3, 2006.

[16] M. S. Vitiello, G. Scamarcio, V. Spagnolo, B. S. Williams, S. Kumar, Q. Hu, and J. L. Reno, "Measurement of subband electronic temperatures and population inversion in THz quantum-cascade lasers," *Appl. Phys. Lett.*, vol. 86, no. 111115, 2005.

[17] C. A. Evans, V. D. Jovanović, D. Indjin, Z. Ikonić, and P. Harrison, "Investigation of thermal effects in quantum-cascade lasers," *IEEE J. Quantum Electron.*, vol. 42, no. 12, pp. 859–867, Dec. 2006.

[18] S. Adachi, *GaAs and Related Materials: Bulk Semiconducting and Superlattice Properties*. Singapore: World Scientific, 1994.

[19] S. Adachi, *Properties of Aluminium Gallium Arsenide*, ser. EMIS Datareviews Series No. 7. London, U.K.: INSPEC, 1993.

[20] A. Lops, V. Spagnolo, and G. Scamarcio, "Thermal modeling of GaInAs–AlInAs quantum cascade lasers," *J. Appl. Phys.*, vol. 100, no. 043109, pp. 1–5, 2006.

[21] D. G. Cahill and R. O. Pohl, "Thermal conductivity of amorphous solids above the plateau," *Phys. Rev. B*, vol. 35, pp. 4067–4073, 1987.

[22] J. C. Brice, *Properties of Indium Phosphide*, ser. EMIS Datareviews Series No. 6. London, U.K.: INSPEC, 1991.

[23] M. S. Vitiello, V. Spagnolo, and G. Scamarcio, "Temperature dependence of thermal conductivity and boundary resistance in thz quantum cascade lasers," *IEEE J. Sel. Topics Quantum Electron*, vol. 14, no. 2, p. 431, Mar./Apr. 2008.
[24] C. Pflügl, M. Litzenberger, W. Schrenk, D. Pogany, E. Gornik, and G. Strasser, "Inferometric study of thermal dynamics in GaAs-based quantum-cascade lasers," *Appl. Phys. Lett.*, vol. 82, no. 11, p. 1664, 2003.
[25] S. T. Huxtable, A. R. Abramson, C. Tien, A. Majumdar, C. LaBounty, X. Fan, G. Zeng, J. E. Bowers, A. Shakouri, and E. T. Croke, "Thermal conductivity of Si–SiGe and SiGe/SiGe superlattices," *Appl. Phys. Lett.*, vol. 80, no. 10, p. 1737, 2002.
[26] S. M. Lee, D. G. Cahill, and R. Venkatasubramanian, "Thermal conductivity of S-Ge superlattices," *Appl. Phys. Lett.*, vol. 70, no. 22, pp. 2957–2959, 1997.
[27] E. T. Swartz and R. O. Pohl, "Thermal boundary resistance," *Rev. Mod. Phys.*, vol. 61, no. 3, p. 605, 1989.
[28] S. S. Howard, Z. Liu, D. Wasserman, A. J. Hoffman, T. S. Ko, and C. Gmachl, "High-performance quantum cascade lasers: Optimized design through waveguide and thermal modeling," *IEEE J. Sel. Topics Quantum Electron.*, vol. 13, no. 5, pp. 1054–1064, Sep./Oct. 2007.
[29] M. S. Vitiello, G. Scamarcio, V. Spagnolo, S. S. Dhillon, and C. Sirtori, "Terahertz quantum cascade lasers with large wall-plug efficiency," *Appl. Phys. Lett.*, vol. 90, no. 191115, pp. 1–3, 2007.
[30] B. S. Williams, "Terahertz quantum-cascade lasers," *Nature Photon*, vol. 1, pp. 517–525, 2007.
[31] J. S. Yu, S. Slivken, S. R. Darvish, A. Evans, B. Gokden, and M. Razeghi, "High-power, room-temperature, and continuous-wave operation of distributed-feedback quantum-cascade lasers at $\lambda \sim 4.8\ \mu$m," *Appl. Phys. Lett.*, vol. 87, no. 041104, p. 1, 2005.

Craig A. Evans was born in Wigan, U.K., in 1982. He received the M.Eng. degree in electronic and photonic communications and the Ph.D. degree in quantum electronics from the University of Leeds, Leeds, U.K., in 2004 and 2008, respectively.

He is currently a Research Assistant in the Institute of Microwaves and Photonics, School of Electronic and Electrical Engineering, University of Leeds, Leeds, U.K., where his research interests include the thermal, optical, and carrier transport properties of quantum-cascade lasers and optical fiber lasers.

Dragan Indjin was born in Zemun, Yugoslavia, in 1963. He received the B.Sc., M.Sc., and Ph.D. degrees in electrical engineering from the University of Belgrade, Belgrade, Yugoslavia, in 1988, 1993, and 1996, respectively.

Since 1989, he has been with the Faculty of Electrical Engineering, University of Belgrade, Belgrade, Yugoslavia, where he is currently Associate Professor. In 2001, he joined the Institute of Microwaves and Photonics, School of Electronic and Electrical Engineering, University of Leeds, Leeds, U.K., where he has recently obtained the prestigious Academic Fellowship. His research interests include the electronic structure, optical and transport properties, optimization and design of quantum wells, superlattices, quantum-cascade lasers, and quantum-well infrared photodetectors from near- to far-infrared spectral range.

Zoran Ikonić was born in 1956 in Belgrade, Yugoslavia. He received the B.Sc., M.Sc., and Ph.D. degrees in electrical engineering from the University of Belgrade, Belgrade, Yugoslavia, in 1980, 1984, and 1987, respectively.

Since 1981, he has been with the Faculty of Electrical Engineering, University of Belgrade, Belgrade, Yugoslavia (Full Professor in 1998). In 1999, he joined the Institute of Microwaves and Photonics, University of Leeds, Leeds, U.K. His research interests include the electronic structure, optical and transport properties of semiconductor nanostructures, and devices based upon them.

Paul Harrison (SM'99) received the B.Sc. degree from the University of Hull, Hull, U.K., in 1988, and the Ph.D. degree from the University of Newcastle-upon-Tyne, U.K., in 1991.

He was a Postdoctoral Research Assistant at the University of Hull until 1995, when he obtained a Fellowship at the University of Leeds, Leeds, U.K. Since joining the Institute of Microwave and Photonics, University of Leeds, he has been working on ways to adapt his theoretical and computational experience in semiconductor heterostructures to terahertz sources and detectors. He currently holds a chair in Quantum Electronics and is Head of the School of Electronic and Electrical Engineering. He is author of the book *Quantum Wells, Wires and Dots, Second Edition* (Wiley, 2005).

Miriam Serena Vitiello was born in Policoro, Italy, in 1978. She received the degree in physics (*cum laude*) in 2001 and the Ph.D. degree in physics from the University of Bari, Bari, Italy, in 2006.

In 2006, she was a Postdoctoral Fellow at CNR-INFM Regional Laboratory LIT3 and since December 2006 she has been a Postdoctoral Fellow at Physics Department, University of Bari. Her research activity concerns the design of quantum-cascade lasers (QCLs) [mid-infrared (MIR) and far-infrared regions], the fabrication of terahertz (THz) and MIR QCLs and the implementation of fabrication techniques for the realization of metal-metal and surface-plasmon THz optical waveguides. She is coauthor of about 40 refereed papers and has delivered 7 invited talks at international conferences.

Dr. Vitiello received one International Scientific Author Award (USA, 2005) and three National Young Author Awards (2003–2005).

Vincenzo Spagnolo was born in Manfredonia, Italy, in 1967. He received the degree in physics and the Ph.D. degree from University of Bari, Bari, Italy, in 1991 and 1994, respectively.

In 1995, he received a fellowship of the National Research Council. In 1996, he received a postdoctoral fellowship from the University of Bari. From 1997-1999, he worked as a Researcher of the National Institute of the Physics of Matter (INFM), Bari. From 1999 to 2003, he was a Postdoctoral Research Associate at the Physics Department, University of Bari. Since January 2004, he has been an Assistant Professor of Experimental Physics at the Politecnico of Bari, Bari, Italy. His main scientific activity has been related to electron-phonon interaction in low-dimensional systems, microprobe optical characterization of semiconductor laser devices, and thermal modeling of Quantum Cascade Lasers. He holds one patent and is author or coauthor of about 75 referred articles and has been an invited speaker in 12 international conferences.

Gaetano Scamarcio (M'95) was born in 1962. He received the Graduate and Ph.D. degrees in physics from the University of Bari, Bari, Italy, in 1985 and 1989, respectively.

He has been a Full Professor of experimental physics at the University of Bari, Bari, Italy, since 1991. From 1989 to 1990, he was a Research Fellow at the Max-Planck-Institute for Festkrperforschung, Stuttgart, Germany, and in 1992, a Visiting Scientist of Walter-Schottky-Institute, Garching, Germany. During 1994-1996, 2000, and 2001 he was a Visiting Scientist of Bell Laboratories, Lucent Technologies, Murray Hill, NJ. In 2006, was Invited Professor at the University of Paris 7. His research interests include: quantum cascade lasers, midinfrared electroluminescence and laser action, development and applications of fiber lasers, spectroscopic techniques for real-time monitoring of optoelectronic devices, optoelectronic sensors for mechatronics. He is author or coauthor of over 130 refereed articles, holds 3 patents, and delivered over 30 invited talks at international conferences.